

Bulk and boundary critical behaviour of thin and thick domain walls in the two-dimensional Potts model

Jérôme Dubail^{1,2}, Jesper Lykke Jacobsen^{2,3} and Hubert Saleur^{1,4}

¹Institut de Physique Théorique, CEA Saclay, 91191 Gif Sur Yvette, France

²LPTENS, École Normale Supérieure, 24 rue Lhomond, 75231 Paris, France

³Université Pierre et Marie Curie, 4 place Jussieu, 75252 Paris, France

⁴Department of Physics, University of Southern California, Los Angeles, CA 90089-0484

E-mail: jerome.dubail@cea.fr, jesper.jacobsen@ens.fr, hubert.saleur@cea.fr

Abstract.

The geometrical critical behaviour of the two-dimensional Q -state Potts model is usually studied in terms of the Fortuin-Kasteleyn (FK) clusters, or their surrounding loops. In this paper we study a quite different geometrical object: the spin clusters, defined as connected domains where the spin takes a constant value. Unlike the usual loops, the domain walls separating different spin clusters can cross and branch. Moreover, they come in two versions, ‘thin’ or ‘thick’, depending on whether they separate spin clusters of different or identical colours. For these reasons their critical behaviour is different from, and richer than, those of FK clusters. We develop a transfer matrix technique enabling the formulation and numerical study of spin clusters even when Q is not an integer. We further identify geometrically the crossing events which give rise to conformal correlation functions. We study the critical behaviour both in the bulk, and at a boundary with free, fixed, or mixed boundary conditions. This leads to infinite series of fundamental critical exponents, $h_{\ell_1-\ell_2, 2\ell_1}$ in the bulk and $h_{1+2(\ell_1-\ell_2), 1+4\ell_1}$ at the boundary, valid for $0 \leq Q \leq 4$, that describe the insertion of ℓ_1 thin and ℓ_2 thick domain walls. We argue that these exponents imply that the domain walls are ‘thin’ and ‘thick’ also in the continuum limit. A special case of the bulk exponents is derived analytically from a massless scattering approach.

PACS numbers: 64.60.De 05.50+q

1. Introduction

Many of the key developments in the study of two-dimensional critical phenomena originate from the study of only a very few lattice models [1, 2]. These include dimer coverings, the Ising and six-vertex models, the $O(n)$ model, and the Q -state Potts model. The latter two models are particularly important, as they can be formulated in terms of geometrical degrees of freedom that in turn describe extended fluctuating objects,

such as domain walls in magnets, percolation clusters, and polymers adsorbed on walls and interfaces [3]. These objects are in fact conformally invariant whenever n or \sqrt{Q} is comprised in the range $-2 < n \leq 2$, and their fluctuations are characterised by critical exponents.

The purpose of this paper is to revisit the geometrical formulation of the two-dimensional Potts model. In particular, we shall define a set of geometrical observables which are different from those considered in most of the existing literature. These observables are simply the domain walls in the formulation of the Potts model in terms of Q -component spins. Not only are they in many ways more natural and physically more relevant than the Fortuin-Kasteleyn (FK) clusters [4] usually considered, but they also turn out to have a richer critical behaviour and a more complete set of critical exponents. These features stem in part from the fact that there are actually two different types of spin domain walls (thin and thick), as we shall explain shortly.

The Q -state Potts model is defined by the partition function

$$Z = \sum_{\sigma} \prod_{(ij) \in E} \exp(K \delta_{\sigma_i, \sigma_j}) , \quad (1)$$

where K is the coupling between spins $\sigma_i = 1, 2, \dots, Q$ along the edges E of some lattice \mathcal{L} . For simplicity we shall take \mathcal{L} to be the square lattice in the computations below, whereas we use the triangular lattice in the figures. The Kronecker delta function $\delta_{\sigma_i, \sigma_j}$ equals 1 if $\sigma_i = \sigma_j$, and 0 otherwise.

The usual route [4] is to write the obvious identity

$$\exp(K \delta_{\sigma_i, \sigma_j}) = 1 + v \delta_{\sigma_i, \sigma_j} , \quad (2)$$

with $v = e^K - 1$, and to expand Z in powers of v . The result is an expression of Z as a sum over FK clusters with weight v per unit length and fugacity Q per connected component. Alternatively one can think of the FK clusters in terms of their surrounding hulls, which are self and mutually avoiding loops with fugacity $n = \sqrt{Q}$ [2]. Most features of these FK clusters and loops, in the critical regime $-2 < n \leq 2$, are by now under complete control, thanks to the combined powers of Conformal Field Theory (CFT) and Schramm-Loewner Evolution (SLE) [5, 6]. In particular, the loops behave like the SLE trace in the continuum limit [6], and viewing them as contour lines of a (deformed) Gaussian free field leads to the Coulomb Gas (CG) approach to CFT [5, 7]. Our understanding of the critical properties of FK clusters and loops can be considered almost complete, although some of their more intricate observables—such as the backbone [8] and shortest-path [9] dimensions—are still unknown.

The expansion in powers of v has some pleasing features, notably that the FK clusters coincide with percolation clusters in the formal limit $Q \rightarrow 1$. But apart from that it is somewhat artificial in view of the original formulation (1) in terms of Q -component spins. In particular, albeit two lattice sites belonging to the same FK cluster will necessarily have the same spin value, the converse is not true. It would therefore seem more natural to perform the expansion in powers of e^K and consider as basic

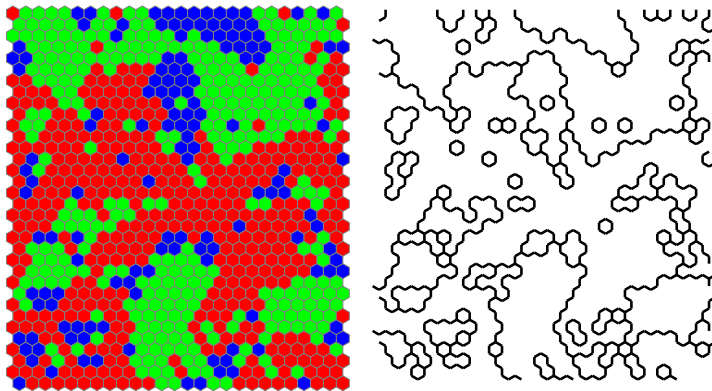


Figure 1. A configuration of the $Q = 3$ Potts model, and the corresponding set of branching domain walls.

geometrical observables the connected domains with a constant value of the Potts spin, henceforth referred to as *spin clusters*.

The properties of these spin clusters have as a rule remained ill understood. This is particularly frustrating, since those are the very clusters that one would observe in an actual experiment on a magnetic alloy in the Potts universality class. The case of the Ising model $Q = 2$ is an exception to this rule [10, 11], but this is due to its “coincidental” equivalence to the $O(n)$ vector model with $n = 1$. Indeed, defining the Ising spins on the triangular lattice, the corresponding $O(n)$ model is described by self and mutually avoiding loops on the hexagonal lattice, and such loops are readily treated by CFT and SLE techniques.

For general Q , the salient feature of Potts spin clusters is that the domain walls separating different clusters undergo branchings and crossings (see Fig. 1). These phenomena are however absent for $Q = 2$ with the above choice of lattice. It is precisely these branchings and crossings that make the application of exact techniques—such as CG mappings or Bethe ansatz diagonalisation—very difficult, if not impossible. The belief that spin clusters are indeed conformally invariant for other values of $Q \neq 2$ in the critical regime has even been challenged at times, but seems however well established by now [12, 13].

Some progress has been accomplished in the $Q = 3$ case [11, 14] by speculating that the spin clusters in the critical Potts model would be equivalent to FK clusters in the *tricritical* Potts model [15, 14]. This equivalence has however not been proven, and is moreover restricted so far to the simplest geometrical questions [16]. The equivalence can also be understood as a relationship with the dilute $O(n)$ model [17].

The Potts model has been used recently to build a new class of 2D quantum lattice models that exhibit topological order [18]. Both FK clusters and domain walls between spin clusters are important in these models. We should also mention that spin domain walls have been studied numerically—and their difference from the FK clusters pointed out—in the context of the Z_N parafermionic models [19].

Apart from issues of branching and crossing, another major hurdle in the study of Potts spin clusters has come from the lack of a formulation that can be conveniently extended to Q a real variable. In the case of loops surrounding the FK clusters, this formulation led naturally to the introduction of powerful algebraic tools via the Temperley-Lieb (TL) algebra, and to the equivalence with the six-vertex model—the eventual key to the exact solution of the problem [5]. Factors of Q then appear naturally through a parameter in the TL algebra, or—via a geometrical construction—as complex vertex weights in the six-vertex formulation. Also for spin clusters can Q be promoted to an arbitrary variable: the weight of a set of spin clusters is simply the chromatic polynomial of the graph dual to the domain walls. From the point of view of the TL algebra, the domain walls are composite (spin-1) objects, hence more complicated than the FK clusters and loops. Recent work on the related Birman-Wenzl-Murakami (BWM) algebra [21, 20] suggests that this formulation might be amenable to the standard algebraic and Bethe ansatz techniques, although such a lofty goal has not been achieved so far.

In this paper we report major progress towards the understanding of Potts spin clusters, both in the bulk and the boundary case. A brief account on the bulk case has recently appeared elsewhere [22]. Our results are of two kinds. On the one hand, we develop a transfer matrix technique which allows the formulation and numerical study of the spin clusters for all real Q . On the other hand, we identify the geometrical events that give rise to conformal correlations, and provide exact (albeit numerically determined) expressions for infinite families of critical exponents, similar to the familiar “ L -legs” exponents [5, 7] for TL loops. Surprisingly, we find that geometrical properties of spin clusters encompass all integer indices (r, s) in the Kac table $h_{r,s}$. An analytical derivation of our results appears for now beyond reach, in part because the algebraic properties of our transfer matrix are still ill understood. We do however provide some exact results based on an approach which does not involve a CG mapping, but rather the use of a massless scattering description.

Apart from the bulk critical exponents [22], we report here the boundary critical exponents for free, fixed, and mixed boundary conditions. This means that the Potts spins on a segment of the boundary are restricted to take Q_1 values, where Q_1 can assume any real value and is in general different from the number of states Q taken by bulk spins. These results can be viewed as a further step in the programme [23] of classifying non-unitary boundary conditions in 2D geometrical models.

2. Domain wall expansion

The domain wall (DW) expansion of (1) involves all possible configurations of domain walls that can be drawn on the dual of \mathcal{L} (see Fig. 2). A DW configuration is given by a graph G (not necessarily connected). The faces of G are the spin clusters. Since we do not specify the colour of each of these clusters, a DW configuration has to be weighted by the chromatic polynomial $\chi_{\hat{G}}(Q)$ of the dual graph \hat{G} . Initially $\chi_{\hat{G}}(Q)$ is defined

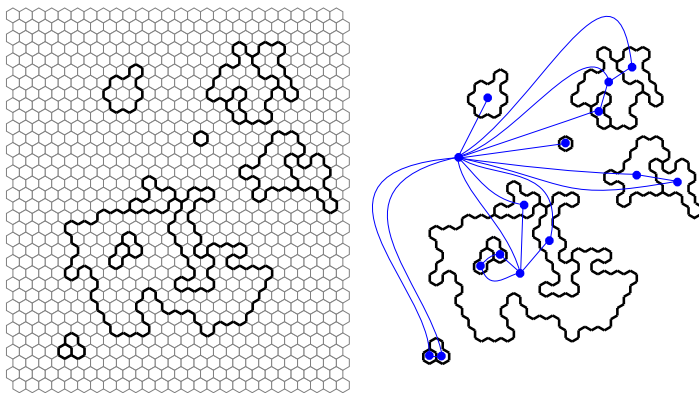


Figure 2. A domain-wall configuration corresponding to a graph G , and its dual graph \hat{G} .

as the number of colourings of the vertices of the graph \hat{G} , using colours $\{1, 2, \dots, Q\}$, with the constraint that neighbouring vertices have different colours. This is indeed a polynomial in Q for any G , and so can be evaluated for any real Q (but $\chi_{\hat{G}}(Q)$ is integer only when Q is integer). For example, the chromatic polynomial of the graph \hat{G} on Fig. 2 is $Q(Q-1)^7(Q-2)^7$. The partition function (1) can thus be written as a sum over all possible DW configurations

$$Z = e^{NK} \sum_G (e^{-K})^{\text{length}(G)} \chi_{\hat{G}}(Q) \quad (3)$$

where N is the number of spins, and $\text{length}(G)$ denotes the total length of the domain walls.

The fundamental geometric object we consider is a connected part of a domain wall that separates two clusters. One can ask how the probability, that a certain number of such DW connect a small (in units of the lattice spacing) neighbourhood A to another small neighbourhood B , decays when the distance x between A and B increases. Each DW separates two spin clusters which connect A and B . There are in fact two types of such DW, depending on the relative colouring of the two clusters that are separated. If the two clusters have different colours, they can touch, so the DW is *thin* (see Fig. 3.a). If the two clusters have the same colour, then they cannot touch (otherwise they would not be distinct), so the DW has to be *thick* (see Fig. 3.b).

Several different geometries are of interest. In the bulk case, the neighbourhoods A and B are at arbitrary, but widely separated, locations in the infinite plane. This is conformally equivalent to an infinitely long cylinder—a strip with periodic boundary conditions—with A and B situated at the two extremities. In the boundary case, the geometry is that of the upper half plane, with A being at the origin and B far away from the real axis. The boundary conditions are taken to be free, fixed or mixed on the positive real axis, and free on the negative real axis. In other words, the Potts spins can take Q_1 (resp. Q) values on the positive (resp. negative) real axis. This geometry is illustrated in Fig. 4; it is conformally equivalent to an infinitely long strip, with A and

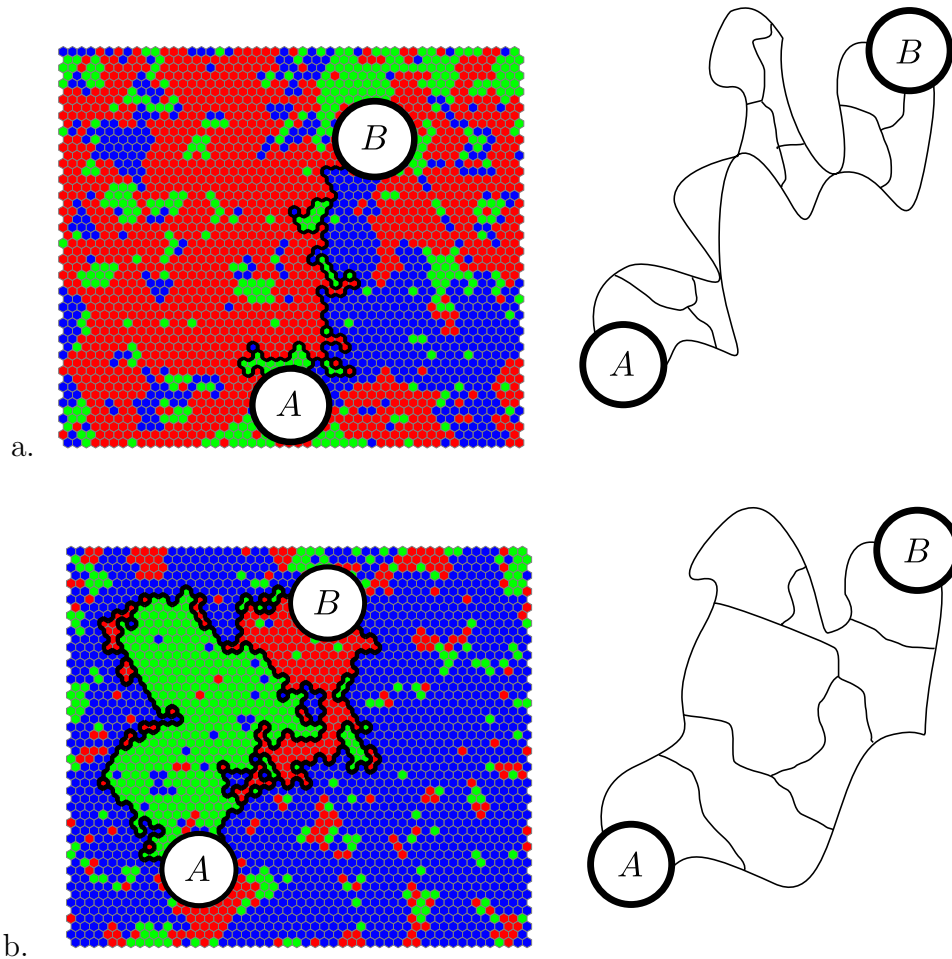


Figure 3. The two different types of DW, here shown in the bulk case (geometry of the infinite plane). A *thin* DW corresponds to the interface between two clusters of different colours (a), while for a *thick* DW the two clusters have the same colour. An illustration for the $Q = 3$ Potts model is given (left) as well as a schematic picture for non-integer Q (right).

B situated at respectively the upper and lower extremities, and spins on the left (resp. right) rim taking Q_1 (resp. Q) values. We shall use the cylinder and strip geometries below to conduct our numerical calculations.

We can now state the central claims of this paper. Consider the 2D Potts model for any real Q in the critical regime $0 \leq Q \leq 4$. Then the probability P that the two regions A and B , with separation $x \gg 1$, are connected by ℓ_1 thin DW and ℓ_2 thick DW decays algebraically. In the bulk case (geometry of the plane) the corresponding critical exponent is denoted $h(Q, \ell_1, \ell_2)$, and we have $P \propto x^{-4h(Q, \ell_1, \ell_2)}$. Equivalently, on a long cylinder of size $L \times \ell$ with $\ell \gg L$, and A and B identified with the opposite ends of the cylinder, the decay is exponential: $P \propto e^{-4\pi(\ell/L)h(Q, \ell_1, \ell_2)}$. In the boundary case (geometry of the half plane) the critical exponent for free boundary conditions is denoted $\tilde{h}(Q, \ell_1, \ell_2)$.

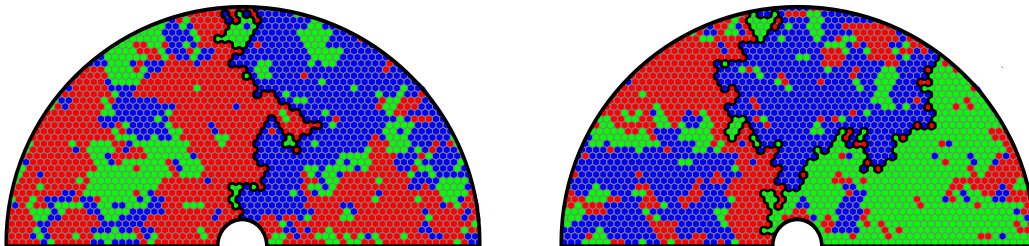


Figure 4. A thin DW in the half plane geometry for $Q = 3$. The left (resp. right) panel illustrates the case where the positive real axis supports free (resp. fixed) boundary conditions.

Below we check these assertions numerically, and we observe that the numerical values of the exponents match the formulae

$$\begin{aligned} h(Q, \ell_1, \ell_2) &= h_{\ell_1 - \ell_2, 2\ell_1}, \\ \tilde{h}(Q, \ell_1, \ell_2) &= h_{1+2(\ell_1 - \ell_2), 1+4\ell_1}, \end{aligned} \quad (4)$$

where we have used the Kac parametrisation of CFT

$$h_{r,s} = \frac{(r - s\kappa/4)^2 - (1 - \kappa/4)^2}{\kappa} \quad (5)$$

and $2 \leq \kappa \leq 4$ parametrises $Q = 4 \left(\cos \frac{\kappa\pi}{4}\right)^2 \in [0, 4]$.

It remains to give our results for the mixed boundary conditions with parameter Q_1 (of which fixed boundary conditions corresponds to the special case $Q_1 = 1$). These follow by conformal fusion of the free-to-mixed boundary condition changing operator Φ_{r_0, s_0} that has been worked out in [23] with the operator $\Phi_{1+2(\ell_1 - \ell_2), 1+4\ell_1}$ that inserts the required number of DW with free boundary conditions. Details about this will be given below in section 5.

We close this section with two remarks about the precise interpretation of the main result (4).

First, in the expression (4) for the bulk exponent $h(Q, \ell_1, \ell_2)$, the case $(\ell_1, \ell_2) = (0, 1)$ of a single DW (which must then necessarily be thick, due to the periodic boundary conditions) is special. In that case (4) remains valid only if the DW is forbidden to wrap around the neighbourhoods A and B (in the geometry of the plane), or around the periodic direction (in the equivalent cylinder geometry). Without that restriction being imposed, we obtain another result:

$$h(Q, 0, 1) = h_{0, 1/2} \quad (\text{wrapping allowed}). \quad (6)$$

Second, in the boundary case the numbers ℓ_1 and ℓ_2 appearing in (4) must be defined more carefully. Indeed, when there are $\ell \equiv \ell_1 + \ell_2$ propagating spin clusters, only the nature ('thin' or 'thick') or the $\ell - 1$ DW separating them is clear by the above definition, whereas it is not yet clear how to characterise the 'half domain walls' that separate the two outermost spin clusters from the boundaries. The correct and unambiguous definition of ℓ_1 and ℓ_2 is as follows: Let the leftmost spin cluster contribute

one unit to ℓ_1 , and let each of the $\ell - 1$ subsequent spin clusters contribute one unit to ℓ_1 (resp. ℓ_2) if it has a different (resp. the same) colour as the cluster on its left.

3. Transfer matrix formulation

The DW expansion (3) may appear unwieldy and difficult to study numerically for non-integer Q . There nevertheless exists several Monte Carlo methods for studying the Potts model when Q is not an integer [24, 25, 26], all of which are roughly speaking based on the FK cluster representation. It is possible to reconstruct the spin clusters from the Chayes-Machta algorithm [25] by performing the bond-adding step at zero temperature. Following our brief account [22], this method has very recently been used [27] to verify a special case of (4) corresponding to $h(Q, 0, 1) = h_{-1,0}$ (with wrapping forbidden).

As in [22] we shall however take a quite different route and resort to a transfer matrix construction. This has the advantage of linking up more easily with CFT [28], and giving very precise numerical results for all the boundary conditions outlined above. Moreover, the ensuing transfer matrix formalism is no more complicated than the one [29] routinely used in the study of the FK clusters.

3.1. State space

Consider a strip of the square lattice of width L spins (boundary conditions will be detailed later). The basis states on which the row-to-row transfer matrix T acts contain one colour label c_i per spin. By definition, one has $c_i = c_j$ if and only if $\sigma_i = \sigma_j$ (i.e., the two spins on sites i and j have the same colour). The colour labels c_i contain less information than the spin colours σ_i themselves. For instance, any configuration in which the first and third spins have the same colour, no matter which one, and no other spins have identical colours, is represented by

$$\begin{array}{ccccccc} c_1 & c_2 & c_1 & c_4 & \dots & c_L \\ \bullet & \bullet & \bullet & \bullet & \dots & \bullet \end{array} \quad (7)$$

With these conventions we are always able to recognise whether two spins have the same colour or not, even if we do not know the precise value of this colour. But this is all that is needed to determine the Boltzmann weights in (1).

For a row of $L = 3$ vertices, and for any (non-integer) Q , there are precisely five basis states

$$\begin{array}{ccccccc} c_1 & c_1 & c_1 & , & c_1 & c_2 & c_1 & , & c_1 & c_1 & c_2 & , & c_1 & c_2 & c_2 & , & c_1 & c_2 & c_3 \end{array} \quad (8)$$

Note that the last state would carry zero weight for $Q = 2$, but apart from that the number of basis states for any given L will be finite and independent of Q .

In general, the number of states is equal to the Bell number B_L of partitions of L objects, with exponential generating function

$$\sum_{L=0}^{\infty} \frac{B_L}{L!} x^L = \exp(e^x - 1). \quad (9)$$

Note that B_L differs from the Catalan number C_L of *planar* partitions, familiar from the FK cluster representation. In particular, $\{1, 2, 1, 2\}$ is a valid state for $L = 4$. For $L \gg 1$ one has asymptotically $C_L \sim 4^L$, whereas B_L grows super-exponentially. When Q is integer, the number of states truncates to $\approx Q^L/Q!$.

Let us take the time evolution direction to be upwards, so that horizontal (resp. vertical) edges are space-like (resp. time-like). We can write T as a product of elementary transfer matrices, each represented symbolically as a rhombus surrounding a single lattice edge, and corresponds to the addition of that edge to the lattice. This edge links spins (shown as solid circles) on diametrically opposite sites of the rhombus. On an $L = 4$ square lattice with periodic boundary conditions this reads

$$T = \begin{array}{c} \bullet & & \bullet & & \bullet & & \bullet & & \bullet \\ & \diagdown & & \diagup & & \diagdown & & \diagup & \\ \bullet & & \bullet & & \bullet & & \bullet & & \bullet \\ & \diagup & & \diagdown & & \diagup & & \diagdown & \\ \bullet & & \bullet & & \bullet & & \bullet & & \bullet \end{array}$$

A rhombus \diamond corresponds to a vertical edge, and acts on a basis state s as follows. If exactly Q_s distinct colour labels $\{c_k\}$ are used in s , then the new colour label c'_i of the spin σ_i can be either unchanged $c'_i = c_i$ (with weight e^K), or any one of the other labels already in use $c'_i = c_k$ (each with weight 1), or a new one $c'_i \notin \{c_k\}$ (with weight $Q - Q_s$). Note that this latter weight is in general non-integer, and is responsible for the correct computation of the chromatic polynomial $\chi_{\hat{G}}(Q)$. On an example with $Q_s = 3$ this reads explicitly

$$\begin{array}{c} \bullet & & \bullet & & \bullet \\ & \diagdown & & \diagup & \\ \bullet & & \bullet & & \bullet \\ & \diagup & & \diagdown & \\ \bullet & & \bullet & & \bullet \end{array} = \delta_{c_3, c'_3} e^K \begin{array}{c} \bullet & \bullet & \bullet \\ c_1 & c_2 & c_3 \end{array} + \delta_{c_1, c'_3} \begin{array}{c} \bullet & \bullet & \bullet \\ c_1 & c_2 & c_1 \end{array} + \delta_{c_2, c'_3} \begin{array}{c} \bullet & \bullet & \bullet \\ c_1 & c_2 & c_2 \end{array} \\ + (1 - \delta_{c_1, c'_3} - \delta_{c_2, c'_3} - \delta_{c_3, c'_3}) (Q - Q_s) \begin{array}{c} \bullet & \bullet & \bullet \\ c_1 & c_2 & c_3 \end{array}$$

The last state could be written $\begin{array}{c} c_1 & c_2 & c'_3 \\ \bullet & \bullet & \bullet \end{array}$, but this is equivalent to $\begin{array}{c} c_1 & c_2 & c_3 \\ \bullet & \bullet & \bullet \end{array}$ in the basis (8).

A rhombus \diamond adding a horizontal edge between vertices i and $i + 1$ corresponds simply to a diagonal matrix, with a weight e^K if $c_i = c_{i+1}$, and 1 otherwise.

With these rules at hand, one can write the periodic (cylinder geometry) $L = 3$ transfer matrix for arbitrary Q in the basis (8) as an instructive example: $T = h_1 \cdot h_2 \cdot h_3 \cdot v_1 \cdot v_2 \cdot v_3$ with

$$v_1 = \begin{pmatrix} e^K & 0 & 0 & 1 & 0 \\ 0 & e^K & 1 & 0 & 1 \\ 0 & 1 & e^K & 0 & 1 \\ Q - 1 & 0 & 0 & e^K + Q - 2 & 0 \\ 0 & Q - 2 & Q - 2 & 0 & e^K + Q - 3 \end{pmatrix}$$

and $h_1 = \text{diag}(e^K, 1, e^K, 1, 1)$. The remaining matrices can be obtained from those given by cyclic permutations of the colour labels:

$$\begin{aligned}
 v_2 &= \begin{pmatrix} e^K & 1 & 0 & 0 & 0 \\ Q-1 & e^K + Q - 2 & 0 & 0 & 0 \\ 0 & 0 & e^K & 1 & 1 \\ 0 & 0 & 1 & e^K & 1 \\ 0 & 0 & Q-2 & Q-2 & e^K + Q - 3 \end{pmatrix} \\
 v_3 &= \begin{pmatrix} e^K & 0 & 1 & 0 & 0 \\ 0 & e^K & 0 & 1 & 1 \\ Q-1 & 0 & e^K + Q - 2 & 0 & 0 \\ 0 & 1 & 0 & e^K & 1 \\ 0 & Q-2 & 0 & Q-2 & e^K + Q - 3 \end{pmatrix} \quad (10)
 \end{aligned}$$

and $h_2 = \text{diag}(e^K, 1, 1, e^K, 1)$, $h_3 = \text{diag}(e^K, e^K, 1, 1, 1)$.

To get a non-periodic strip geometry instead of a periodic cylinder, one needs simply to omit the last horizontal edge which is responsible for the periodic boundary conditions. For instance, with $L = 3$ one would have $T = h_1 \cdot h_2 \cdot v_1 \cdot v_2 \cdot v_3$. This corresponds to free boundary conditions. Mixed boundary conditions are obtained by constraining the spins on the left boundary of the strip to belong to a subset of Q_1 different colours, with $0 < Q_1 \leq Q$. Spins on the right boundary remain free. For Q_1 integer this can be coded in the transfer matrix by considering that the number of colours in use in a given state is always at least Q_1 (so that in particular $Q_s \geq Q_1$). These first Q_1 colours are considered fixed, whereas other colours $Q_1 + 1, Q_1 + 2, \dots$ are defined only relative to the fixed ones, as described above. In particular, the choice $Q_1 = 1$ corresponds to fixed boundary conditions.

The leading eigenvalue Λ_0 of the transfer matrix T with periodic boundary conditions gives the ground state free energy $f_0 = -\frac{1}{L} \log \Lambda_0$. This f_0 coincides precisely with that of the usual FK transfer matrix [29], even when Q is non-integer.‡ Its finite-size corrections possess a universal L^{-2} term whose coefficient determines the central charge of the corresponding CFT [28].

3.2. Correlation functions

However, to obtain the desired two-point correlation functions of DW, we need to construct a variant transfer matrix T_{ℓ_1, ℓ_2} which imposes the propagation of ℓ_1 thin and ℓ_2 thick DW along the time direction of the cylinder (or strip). From its leading eigenvalue Λ_{ℓ_1, ℓ_2} one can determine the energy gap $\Delta f_{\ell_1, \ell_2} = -\frac{1}{L} \log(\Lambda_{\ell_1, \ell_2} / \Lambda_0)$ whose finite-size scaling in turn determines the critical exponents $h(Q, \ell_1, \ell_2)$ and $\tilde{h}(Q, \ell_1, \ell_2)$ [28, 5].

To this end, the basis states (8) need to be endowed with some additional information about the connectivity of the spin clusters, ensuring the propagation of the

‡ The reader may wish to check this fact on the $L = 3$ example given above.

desired number and types of DW. The crucial point is that we need to know whether two spins having the same colour label c_i also belong to the same cluster. Thus the states we use in the final transfer matrix have the form

$$\begin{array}{c}
 c_1 \quad c_2 \quad c_1 \quad c_1 \quad c_5 \\
 \bullet \quad \bullet \quad \cup \quad \bullet \quad \bullet \\
 \\
 c_1 \quad c_2 \quad c_1 \quad c_1 \quad c_5 \\
 \bullet \quad \bullet \quad \cup \quad \cup \quad \bullet
 \end{array}
 \tag{11}$$

meaning that two spins belong to the same spin cluster if and only if they are linked up in this pictorial representation. Of course, only spins with a common colour label can be linked up. Thus, in the left state of (11), the spins on vertices 3 and 4 are in the same cluster, but not in the same cluster as the spin 1. In the right state the spins 1, 3 and 4 are all in the same cluster. These two states are different. In the transfer matrix evolution, each time two neighbour vertices correspond to the same colour, the corresponding clusters are linked up.

Note that the possible ways of linking up the spins must respect planarity. For instance, in the $L = 4$ state with colour labels $\{1, 2, 1, 2\}$, one cannot simultaneously link the first and third spins, and the second and fourth, since this possibility is disallowed by planarity.

To construct T_{ℓ_1, ℓ_2} we modify the linked basis states (11) so that precisely $\ell_1 + \ell_2$ spin clusters are *marked*. The colour labels of the marked clusters must respect the chosen values of ℓ_1 and ℓ_2 . In order to conserve the marked clusters in the transfer matrix evolution, none of the marked clusters must be “left behind”, and two distinct marked clusters must not be allowed to link up. When a marked and an unmarked cluster link up, the result is a marked cluster.

To summarise, the final transfer matrix thus keeps enough information, both about the mutual colouring of the sites and about the connectivity of the clusters, to give the correct Boltzmann weights to the different configurations, even for non-integer Q , and to follow the evolution of the boundary of a particular set of clusters. These boundaries are precisely the domain walls (see Fig. 3).

4. Numerical results

We have numerically diagonalised the transfer matrix in the DW representation for cylinders and strips of width up to $L = 11$ spins. We verified that the leading eigenvalue Λ_0 in the ground state sector coincides with that of the FK transfer matrix, including for non-integer Q . As to the excitations Λ_{ℓ_1, ℓ_2} , we explored systematically all possible colouring combinations for up to 4 marked spin clusters, for a variety of values of the parameter κ , and for several different boundary conditions (periodic, free, fixed, and mixed).

Finite-size approximations of the critical exponents $h(L)$ and $\tilde{h}(L)$ were extracted from the leading eigenvalue in each sector, using standard CFT results [28, 5], and fitting both for the universal corrections in L^{-2} and the non-universal L^{-4} term. These approximations were further extrapolated to the $L \rightarrow \infty$ limit by fitting them to first

$p = \frac{\kappa}{4-\kappa}$	(2, 0)	(0, 2)	(3, 0)	(2, 1)	(0, 3)	(0, 1)*
2	2.01(1)	5.99(2)	2.97(4)		8.94(2)	1.000(0)
3	4.01(1)	7.99(2)	6.02(2)	8.04(2)	11.98(3)	1.500(1)
4	5.93(2)	10.01(2)	8.89(5)	10.93(5)	15.05(4)	1.992(2)
5	7.77(4)	12.09(8)	11.6 (1)	13.8 (1)	18.2 (2)	2.47 (2)
Exact	$2(p-1)$	$2(p+1)$	$3(p-1)$	$3p-1$	$3(p+1)$	$p/2$

Table 1. Bulk critical exponents corresponding to five different DW configurations (ℓ_1, ℓ_2) , as functions of the parameter $p = \frac{\kappa}{4-\kappa}$, along with the conjectured exact expression (4). The last column labelled $(0, 1)^*$ is for a single DW which is allowed to wrap around the periodic direction. The table entries give the value of $|\rho|$, when (5) is rewritten as $h_{r,s} = (\rho^2 - 1)/(4p(p+1))$, with error bars shown in parentheses.

$p = \frac{\kappa}{4-\kappa}$	(2, 0)	(1, 2)	(2, 1)	(3, 0)
3	7.00(3)	19.0(2)	15.16(4)	11.13(4)
4	10.89(7)	24.8(2)	20.9 (1)	16.74(5)
5	14.5 (1)	31.1(2)	26.7 (2)	22.2 (3)
Exact	$4p-5$	$6p+1$	$6p-3$	$6p-7$

Table 2. Boundary critical exponents with free boundary conditions, corresponding to four different DW configurations (ℓ_1, ℓ_2) , as functions of the parameter $p = \frac{\kappa}{4-\kappa}$, along with the conjectured exact expression (4). The table entries give the value of $|\rho|$, when (5) is rewritten as $h_{r,s} = (\rho^2 - 1)/(4p(p+1))$, with error bars shown in parentheses.

and second order polynomials in L^{-1} , gradually excluding data points corresponding to the smallest L . Error bars were obtained by carefully comparing the consistency of the various extrapolations.

Representative final results for the bulk case (periodic boundary conditions) are shown in Table 1. Recall that (4) is only valid for $(\ell_1, \ell_2) = (0, 1)$ if the spin cluster is forbidden to wrap around the periodic direction. The sector where such wrapping is allowed is denoted $(0, 1)^*$ in Table 1, and the corresponding critical exponent turns out to be $h_{0,1/2}$.

Final results for the boundary case with free boundary conditions are shown in Table 2. The convention for the labels (ℓ_1, ℓ_2) is the one stated below Eq. (6).

5. Mixed boundary conditions

We recall that mixed boundary conditions have been defined by imposing that the spins on the left boundary of the strip belong to a subset of Q_1 different colours, with $0 < Q_1 \leq Q$, while the spins on the right boundary remain free. In particular, $Q_1 = 1$ (resp. $Q_1 = Q$) describes fixed (resp. free) boundary conditions. As above, the convention for the labels (ℓ_1, ℓ_2) is the one stated below Eq. (6).

An important point is that the fixed colour of the leftmost marked spin cluster may or may not be one of those allowed on the left boundary. For each choice of colours of the marked clusters, we define a sign $\epsilon = 1$ (resp. $\epsilon = -1$) if the colour of the leftmost cluster is $k_1 \leq Q_1$ (resp. $k_1 > Q_1$), i.e., if the leftmost cluster is allowed to (resp. not allowed to) touch the left boundary. This sign closely parallels a construction in [23], where the case $\epsilon = 1$ (resp. $\epsilon = -1$) was referred to as the blobbed (resp. unblobbed) sector. For free boundary conditions, only the choice $\epsilon = 1$ is meaningful (at least for $0 < Q_1 \leq Q$, although it might be possible to give a meaningful definition of the model outside this range, by a suitable analytical continuation). The issue of the sign $\epsilon = \pm 1$ is illustrated in Fig. 5.

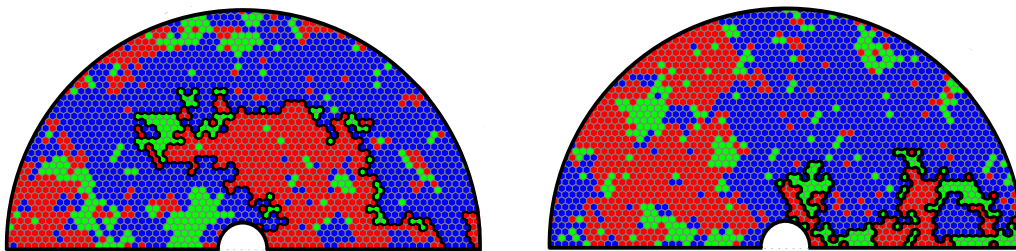


Figure 5. Mixed boundary conditions in the half plane geometry for $Q = 3$ and $Q_1 = 2$. The left (resp. right) panel illustrates the case $\epsilon = 1$ (resp. $\epsilon = -1$) where the propagating cluster, shown in blue colour, is allowed to (resp. not allowed to) touch the positive real axis.

One would expect the mixed boundary conditions to be given by the conformal fusion of the operator $\Phi_{1+2(\ell_1-\ell_2),1+4\ell_1}$ that inserts the required number of DW, and the free-to-mixed boundary condition changing operator Φ_{r_0,s_0} . The latter operator is responsible for the shift from Q to Q_1 allowed colours on the boundary. It has been worked out in [23] in the context of a different set of geometrical observables (TL loops), but since it should be representation-independent we can take it over here. The dominant exponents for mixed boundary conditions therefore follow from the standard CFT fusion rules [5] as

$$h_{r_0+2\epsilon(L_1-L_2),s_0+4\epsilon L_1}, \quad (12)$$

where h_{r_0,s_0} is the dimension of the free-to-mixed boundary condition changing operator Φ_{r_0,s_0} .

The values of (r_0, s_0) follow from [23], e.g., $(-1, -2)$ for $Q_1 = 1$ and $(-\frac{1}{2}, -1)$ for $Q_1 = 2$. We have verified these and other cases by explicit numerical calculations. In particular, the possible ambiguity of ϵ versus $-\epsilon$ in (12) is ruled out by the numerical results. Moreover (12) agrees with (4) for free boundary conditions ($\epsilon = 1$) as it should.

6. Massless scattering description

While it is far from obvious to derive (4) by CG methods, minor progress can be achieved using a rather different set of ideas. We restrict the discussion in this section to the bulk properties.

We can learn about the dynamics of DW in the critical theory by using known information about the low-temperature ($K > K_c$) phase of the Potts model. Albeit non-integrable on the lattice, the corresponding deformation by the operator Φ_{21} is integrable in the continuum [30]. It can be described using a basic set of kinks K_{ab} separating two vacua, i.e., ordered regions where the dominant value of the spin is a , resp. b . These kinks scatter with a known S-matrix related to the BWM algebra [21]. Importantly, the dynamics conserves the number of kinks: the process $K_{ab}K_{bc} \rightarrow K_{ac}$ is forbidden (as in any elastic relativistic scattering theory), although kinks do appear as bound states in kink-kink processes.

Many properties of these kinks can be calculated using integrability techniques. When the mass $m \rightarrow 0$ (i.e., $K \rightarrow K_c$), the S-matrix provides a “massless scattering” description [31] of some of the degrees of freedom of the critical theory itself. It is not entirely clear what a kink, which is well-defined for $K \gg K_c$, becomes at K_c , but it is natural to expect that thick DW are described by the propagation of two (or more) kinks such as $K_{ab}K_{ba}$. As for thin DW, the potential existence of regions where they are reduced to a single edge—that is a single kink—suggest they have to do with more complicated processes involving two kinks merging into one. We will not discuss them further here.

It is an easy exercise to obtain the scaling dimension of thick DW using the massless scattering description. Indeed, the fact that the S-matrix satisfies relations from the BWM algebra allows us to reexpress it in terms of the $a_2^{(2)}$ or Bullough-Dodd S-matrix [32], for which the thermodynamic Bethe ansatz was studied in [33]. This describes as well the dynamics of the field theory

$$S = \frac{1}{8\pi} \int d^2x \left[(\partial_x \Phi)^2 + (\partial_y \Phi)^2 + g(2e^{-\frac{i}{\sqrt{2}}\beta\Phi} + e^{i\sqrt{2}\beta\Phi}) \right] \quad (13)$$

with $\beta^2 = \frac{\kappa}{4}$. Giving each kink the fugacity $Q - 1$ produces the correct central charge

$$c = 1 - \frac{3(\kappa - 4)^2}{2\kappa}, \quad (14)$$

where each kink has a $U(1)$ charge equal to $0, \pm 1$. The scaling of the sector with charge j produces a gap $\Delta_j = \frac{j^2}{4\kappa}$, so the leading dimension is $\Delta_j - (1 - c)/24 = h_{j/2,0}$. This agrees with $h_{-\ell_2,0}$ with $\ell_2 = j/2$, so there are two kinks per thick DW.

This argument validates (4) for $\ell_1 = 0$.

7. Discussion

The results (4) and (6) can be used to predict the fractal dimension of various geometrical objects related to spin clusters. It should be possible to observe these dimensions in

Monte Carlo simulations, and possible in real experiments.

7.1. Fractal dimensions

The dimension of a spin cluster follows from (6) as

$$\begin{aligned} d &= \min(2, 2 - 2h_{0,1/2}) \\ &= \begin{cases} 2 & \text{for } \kappa \in [2, \frac{8}{3}] \\ \frac{(8+\kappa)(8+3\kappa)}{32\kappa} & \text{for } \kappa \in [\frac{8}{3}, 4] \end{cases} \end{aligned} \quad (15)$$

in agreement with [10, 11].

The boundary of a spin cluster has dimension

$$d_b = 2 - 2h_{-1,0} = 1 + \frac{\kappa}{8}. \quad (16)$$

This is an example of a duality relation: d_b for a spin cluster with SLE parameter κ equals the dimension d_b^{FK} of the boundary of an FK cluster at the dual parameter $\kappa^* = \frac{16}{\kappa}$. It is moreover known that d_b^{FK} at parameter κ coincides with the dimension d_b^{EP} of the FK cluster's external perimeter (with fjords filled in) at parameter κ^* [16]. Combining these, (16) means that $d_b = d_b^{\text{EP}}$, i.e., the dimension of the boundary of a spin cluster equals that of the external perimeter of an FK cluster, at the same κ . This latter fact has very recently been verified numerically by Monte Carlo simulations, including for non-integer values of Q [27].

In the half-plane geometry, the intersection of the spin cluster containing the origin with the real axis has the dimension

$$d_s = \min(1, 1 - h_{3,5}) = \min\left(1, 8 - \frac{8}{\kappa} - \frac{3\kappa}{2}\right), \quad (17)$$

as follows from (4).

7.2. Thin and thick domain walls

We have initially attached the epithets ‘thin’ and ‘thick’ to the two types of domain walls based on considerations in the microscopic model. Indeed, thin DW can narrow down to a single lattice edge on the dual lattice, separating spins of different colour. Since (4) implies that the two types of DW scale differently in the continuum limit, one would expect that also the continuum geometrical objects can somehow be characterised as ‘thin’ and ‘thick’. We now show that this is indeed the case.

According to (4), the set of points where a thin DW has minimal width—i.e., one lattice spacing in the microscopic formulation, or the two clusters separated by the DW ‘come close’ in the continuum limit in the sense of the small neighbourhoods defined previously—has dimension

$$d_1 = 2 - 2h_{2,4} = \frac{3}{8\kappa}(4 - \kappa)(5\kappa - 4). \quad (18)$$

This is analogous to the dimension of so-called ‘red’ or ‘pivotal’ bonds in the theory of percolation and of FK clusters. The corresponding result for a thick DW reads

$$d_2 = \max(0, 2 - 2h_{-2,0}) = 0. \quad (19)$$

The fact that $d_1 \geq 0$ means that thin DW are indeed thin, in the sense that they have a macroscopic number of loci of zero thickness in the continuum limit. Likewise, the fact that $d_2 = 0$ means that the loci where thick DW have zero thickness is a set of measure zero.

To summarise, there is therefore a consistency between the distinction of the two types of DW microscopically and in the continuum limit, and this ensures that they can (and do) scale differently.

One can also obtain dimensions analogous to d_1 and d_2 at the boundary. Indeed, define \tilde{d}_1 (resp. \tilde{d}_2) to be the fractal dimension of the set which is the intersection of the real axis with the set of points where a thin (resp. thick) DW has minimal width. In other words, these are the dimensions of pivotal bonds on the boundary. By setting $\ell_1 = 2$ and $\ell_2 = 0$ (resp. $\ell_1 = 0$ and $\ell_2 = 2$) in (4) we have then

$$\begin{aligned} \tilde{d}_1 &= \min(1, \max(0, 1 - h_{5,9})) \\ &= \begin{cases} 1 & \text{for } \kappa \in [2, \frac{12}{5}] \\ \frac{1}{\kappa}(3 - \kappa)(5\kappa - 8) & \text{for } \kappa \in [\frac{12}{5}, 3] \\ 0 & \text{for } \kappa \in [3, 4] \end{cases} \end{aligned} \quad (20)$$

respectively

$$\tilde{d}_2 = \max(0, 1 - h_{-3,1}) = 0. \quad (21)$$

7.3. The limit $Q = 4$

In the limit $Q \rightarrow 4$ (or $\kappa \rightarrow 4$), we have $d_1 \rightarrow 0$ and $d_2 \rightarrow 0$. This means that the distinction between thin and thick DW disappears in that limit. This is of course consistent with the fact that $\kappa = 4$ is a fixed point of the duality transformation $\kappa^* = \frac{16}{\kappa}$, and so spin clusters and FK clusters have identical properties.

A further manifestation of the indistinguishability of thin and thick DW is that the bulk exponent (4) becomes

$$h_{\ell_1 - \ell_2, 2\ell_1} = \frac{(\ell_1 + \ell_2)^2}{4}. \quad (22)$$

Indeed, this formula is invariant under the permutation of ℓ_1 and ℓ_2 . Moreover, the exponent for ℓ FK clusters reads $\frac{\ell^2}{4}$ for $Q = 4$ [5, 7], and so a spin DW (whether thin or thick) behaves as a FK cluster, as expected.

7.4. The case $Q = 2$

For the Ising model $Q = 2$ (or $\kappa = 3$) the absence of branchings means that one thick DW equals two thin DW. Indeed the bulk exponent becomes (4) becomes

$$h_{\ell_1 - \ell_2, 2\ell_1} = \frac{4\ell^2 - 1}{48} \quad (23)$$

with $\ell = \ell_1 + 2\ell_2$ in that case, and this agrees with the exponent $h_{\ell/2,0}$ for ℓ loop strands [5, 7] in the dilute $O(1)$ model.

7.5. The limit $Q \rightarrow 1$

The limit $Q \rightarrow 1$ (or $\kappa \rightarrow \frac{8}{3}$) is often studied in the context of FK clusters, since these become then bond percolation clusters. Setting $Q = 1$ for spin clusters has a more trivial meaning: all the spins are simply in the same state, $\sigma_i = 1$. Therefore we should have $d = 2$ and d_s for $Q \rightarrow 1$. This is indeed satisfied by (15) and (17).

Apart from that, the $Q \rightarrow 1$ limit for spin clusters is more subtle. One can tackle it by considering configurations of bond percolation on the square lattice where one picks up *one* single percolation cluster. The spins on the vertices sitting on this cluster are given a certain colour. All the other spins in the system are given another single colour. Then the boundary of the coloured *spin* cluster is a single loop with fractal dimension $d_f = 4/3$, as expected from the duality $\kappa^* = 16/\kappa$. It is, however, remarkable that we can find such a simple construction of the *spin* cluster for $Q = 1$ on the lattice. For more interfaces one has to pick up more percolation clusters, and give them different colours.

Finally, we note that for $Q = 1$ we have

$$h_{\ell_1 - \ell_2, 2\ell_1} = \frac{\ell^2 - 1}{24}, \quad (24)$$

which agrees with $h_{0,\ell/2}$ if one sets $\ell = \ell_1 + 3\ell_2$. This seems to indicate that for percolation, a thick DW equals *three* thin DWs (or TL loop strands)—a curious result for which we have no convincing explanation at present.

8. Conclusion

We have defined a set of geometrical observables based on the branching domain walls of the Potts model for any real $0 \leq Q \leq 4$. These observables are defined starting from the DW expansion (3) of the partition function. We have studied numerically these objects for non-integer Q using a transfer matrix formulation. Our results are compatible with conformal invariance of these observables and we have given a set of conjectures for the corresponding bulk and boundary critical exponents.

Acknowledgments

We thank G. Delfino and P. Fendley for discussions. This work was supported by the Agence Nationale de la Recherche (grant ANR-06-BLAN-0124-03).

References

- [1] F.Y. Wu, *Exactly solved models: A journey in statistical mechanics* (World Scientific, Singapore, 2008).

- [2] R.J. Baxter, *Exactly solved models in statistical mechanics* (Academic Press, London, 1982).
- [3] E. Eisenriegler, *Polymers near Surfaces* (World Scientific, Singapore, 1993).
- [4] C.M. Fortuin and P.W. Kasteleyn, *Physica* **57**, 536 (1972).
- [5] J.L. Jacobsen, *Lect. Notes Phys.* **775**, 347–424 (2009).
- [6] M. Bauer and D. Bernard, *Phys. Rep.* **432**, 115 (2006).
- [7] B. Nienhuis, *Loop Models*, Les Houches Summer School: Volume 89, July 2008. (Oxford University Press, 2010)
- [8] Y. Deng, H.W.J. Blöte and B. Nienhuis, *Phys. Rev. E* **69**, 026114 (2004).
- [9] Y. Deng, W. Zhang, T.M. Garoni, A.D. Sokal and A. Sportiello, *Phys. Rev. E* **81**, 020102(R) (2010).
- [10] B. Duplantier and H. Saleur, *Phys. Rev. Lett.* **63**, 2536 (1989).
- [11] C. Vanderzande, *J. Phys. A* **25**, L75 (1992).
- [12] A. Coniglio and F. Peruggi, *J. Phys. A* **15**, 1873 (1982).
- [13] X. Qian, Y. Deng and H.W.J. Blöte, *Phys. Rev. B* **71**, 144303 (2005).
- [14] W. Janke and A. Schakel, *Braz. J. Phys.* **36**, 708 (2006); *Phys. Rev. E* **71**, 036703 (2005); *Nucl. Phys. B* **700**, 385 (2004).
- [15] A.L. Stella and C. Vanderzande, *Phys. Rev. Lett.* **62**, 1067 (1989); *J. Phys. A* **22**, L445 (1989).
- [16] B. Duplantier, *Phys. Rev. Lett.* **84**, 1363 (2000).
- [17] A. Gamsa and J. Cardy, *J. Stat. Mech.* P08020 (2007).
- [18] P. Fendley, *Annals of Physics* **323**, 3113 (2008).
- [19] M. Picco, R. Santachiara and A. Sicilia, *J. Stat. Mech.* (2009) P04013; M. Picco and R. Santachiara, arXiv:1005.0493.
- [20] P. Fendley, *J. Phys. A* **39**, 15445 (2006).
- [21] P. Fendley and N. Read, *J. Phys. A* **35**, 10675 (2002).
- [22] J. Dubail, J.L. Jacobsen and H. Saleur, arXiv:1008.1216.
- [23] J.L. Jacobsen and H. Saleur, *Nucl. Phys. B* **788**, 137 (2008); J. Dubail, J.L. Jacobsen and H. Saleur, *Nucl. Phys. B* **813**, 430 (2009); *ibid.* **827**, 457 (2010).
- [24] M. Sweeny, *Phys. Rev. B* **27**, 4445 (1983).
- [25] L. Chayes and J. Machta, *Physica A* **254**, 477 (1998).
- [26] Y. Deng, X. Qian and H.W.J. Blöte, *Phys. Rev. E* **80**, 036707 (2009).
- [27] A. Zatelepin and L. Shchur, arXiv:1008.3573.
- [28] H.W.J. Blöte, J.L. Cardy and M.P. Nightingale, *Phys. Rev. Lett.* **56**, 742 (1986).
- [29] H.W.J. Blöte and M.P. Nightingale, *Physica A* **112**, 405 (1982).
- [30] L. Chim and A. Zamolodchikov, *Int. J. Mod. Phys. A* **7**, 5317 (1992).
- [31] P. Fendley and H. Saleur, in Gava *et al.* (eds.), *Proceedings of the Trieste Summer School in High Energy Physics and Cosmology* (World Scientific, 1993).
- [32] C.J. Efthimiou, *Nucl. Phys. B* **398**, 697 (1993).
- [33] H. Saleur and B. Wehefritz-Kaufmann, *Nucl. Phys. B* **628**, 407 (2002).